Nanoscale

Ozone-mediated synthesis of ceria nanoparticles

Journal:	*Nanoscale*
Manuscript ID	NR-COM-03-2018-001971.R1
Article Type:	Communication
Date Submitted by the Author:	21-Apr-2018
Complete List of Authors:	Bhalkikar, Anuja; University of Nebraska-Lincoln, Department of Chemistry Wu, Tai-Sing; National Tsing Hua University, Physics Marin, Chris; University of Nebraska at Lincoln, Chemistry Fisher, Tamra; University of Nebraska-Lincoln, Chemistry Wang, Meiyu; University of Nebraska-Lincoln Wells, Isaac; University of Nebraska-Lincoln Sarella, Anandakumar; University of Nebraska-Lincoln Soo, Yun Liang; National Tsing Hua University, Physics Cheung, Barry; University of Nebraska-Lincoln

Nanoscale

COMMUNICATION

Ozone-mediated synthesis of ceria nanoparticles

Anuja Bhalkikar,[a] Tai-Sing Wu,[b] Chris M. Marin,[a] Tamra. J. Fisher,[a] Meiyu Wang,[c] Isaac H. Wells,[a] Anandakumar Sarella,[d] Yun-Liang Soo,[b, e] and Chin Li Cheung[a*]

Received 00th January 20xx,
Accepted 00th January 20xx

DOI: 10.1039/x0xx00000x

www.rsc.org/

We report a rapid, room temperature methodology to synthesize fluorite-structured ceria nanoparticles using cerium (III) salts and ozone in the presence of short chain primary, secondary, and tertiary alcohols. This simple technique produced nanoparticles with higher oxygen vacancy compared to that of bulk ceria.

Introduction

Fluorite-structured cerium oxide (ceria, CeO_x: x = 1.5 to 2) is one of the most versatile lanthanide oxides with market worth in the U.S. estimated at USD 84.6 million in 2016.[1] It has widespread industrial applications in oxygen sensors, solid oxide fuel cells, UV blockers, optical devices, polishing materials and biomedicine.[2] Intrinsic oxygen vacancy defects in conjunction with the reversible cycling of Ce^{3+} and Ce^{4+} and large surface areas make nanosized ceria an efficient catalyst compared to its bulk counterparts in organic chemical synthesis.[3] The wide-ranging demand for this material has resulted in the development of numerous synthetic methodologies including sol-gel synthesis, solvothermal synthesis, hydrothermal synthesis, hydrolysis, and chemical precipitation.[4, 5] In general, these techniques are not energy-efficient. They require either long reaction times, elevated temperatures, and/or high pressures. Some reported methods employ expensive metal alkoxides and caustic alkalis[5] which necessitate the need for inexpensive and safer synthetic procedures.

Milder wet chemical techniques utilizing strong oxidants such as hydrogen peroxide in the presence of a base have been explored for ceria nanoparticles (NPs) generation. However, these methodologies not only need an additional step to convert cerium hydroxide to cerium oxide but also require nanoparticle stabilizers.[6] Recently, a room-temperature peroxide-based synthetic route with various cerium salts was demonstrated for ceria NPs development. Although this method produced ceria NPs with a higher surface Ce^{3+} percentage, a stabilization time of 30 days was required to obtain a stable dispersion of these particles.[7]

Reported uses of ozone for the syntheses of metal oxide microstructures and nanostructures have been sparse. Tolstoi *et al* demonstrated the synthesis of birnessite microtubes from aqueous manganese acetate under an ozone environment.[8] However, no thorough investigation of the growth of these microtubes was conducted in the study. Recently, Morris *et al* pioneered a block copolymer assisted method to fabricate Ce_2O_3-like nanodots with UV/ozone. In this method, ethanol solutions of cerium (III) salts were spin-coated on block copolymer films, which were then subjected to UV/ozone treatment to generate 20-nm nanodots. Subsequent UV/ozone exposure was employed to completely remove polymer residues from the products and cause the partial oxidation of Ce^{3+} to Ce^{4+} in these nanodots.[9] To our best knowledge, direct use of ozone to synthesize ceria nanoparticles in solution has not yet been reported or demonstrated.

Herein we report a rapid, room-temperature and hydroxide-free method of fluorite-structured ceria NPs synthesis using ozone and inexpensive, aliphatic alcohols. Ceria NPs of average size ranging from 2 nm to 4 nm were produced under 15 seconds of bubbling ozone into the alcohol-cerium salt solutions. The NP size distribution was found not affected by longer ozonation processes. Studies of the atomic structures and optical properties of these NPs revealed a high disorder in their lattice structures. The effects of primary, secondary, and tertiary alcohols and cerium (III) salts of different anions on ceria NPs synthesized with ozone were also evaluated. Chemical species in the reaction mixtures were also studied to elucidate a possible growth mechanism of these nanoparticles from ozonating alcoholic solutions of cerium

[a] *Department of Chemistry, University of Nebraska-Lincoln, Lincoln, Nebraska 68588, United States. Email:ccheung2@unl.edu*
[b] *National Tsing Hua University, Hsinchu 30013, Taiwan, R.O.C.*
[c] *Department of Mechanical and Materials Engineering, University of Nebraska-Lincoln, Lincoln, Nebraska 68588, United States.*
[d] *Nebraska Center for Materials and Nanoscience, University of Nebraska-Lincoln, Lincoln, Nebraska 68588, United States.*
[e] *National Synchrotron Radiation Research Centre, Hsinchu 30076, Taiwan, R.O.C.*
Electronic Supplementary Information (ESI) available: Characterization details of samples made with different precursors and solvents. See DOI: 10.1039/x0xx00000x

salts. The catalytic activity of ceria NPs towards the oxidation of carbon monoxide (CO) was also evaluated and compared with that of a commercial bulk ceria.

Experimental

2.1 Materials

Cerium (III) nitrate hexahydrate ($Ce(NO_3)_3.6H_2O$, REacton, 99.99%), cerium (III) chloride heptahydrate ($CeCl_3{\cdot}7H_2O$, 99%) and commercial bulk cerium (IV) oxide (CeO_2, REacton, 99.9% REO) were purchased from Alfa Aesar (Tewksbury, MA). 200-proof ethanol was purchased from Fisher Scientific (Waltham, MA). Methanol (HiPerSolv CHROMANORM® gradient for HPLC) and 0.2-µm PTFE syringe filters were obtained from VWR Chemicals (Radnor, PA). 2-propanol (ACS reagent, ≥99.5%), tert-butanol (anhydrous, ≥99.5%), and deuterated chloroform ($CDCl_3$, 99.8 atom% D) were purchased from Sigma-Aldrich (St. Louis, MO). Poly-*L*-lysine (0.1% w/v) was obtained from Ted Pella (Redding, CA). All purchased chemicals were used without further purification.

2.2 Synthesis of ceria nanoparticles

Ceria nanoparticles (ceria NPs) were synthesized by bubbling solutions of different cerium salts in alcohols with ozone for 15 sec, 5 min, 30 min and 1 h. Typically, 0.5 g of $Ce(NO_3)_3{\cdot}6H_2O$ was dissolved in 20 mL of 200-proof ethanol. The salt solution was bubbled for 30 min with a stream of ozone (0.5 g/h) generated by passing 200 SCCM of extra dry oxygen (99.6%, Matheson Tri-Gas, Lincoln, NE) through an ozone generator (MP-3000, A2Z Ozone, Louisville KY). The reaction solution changed from a clear solution to a yellow-orange cloudy solution with orange-red precipitates. The mixture was centrifuged at 4500 RPM for 20 min. The precipitate pellet was resuspended in a fresh aliquot of ethanol and centrifuged again using the same parameters. The resulting orange-red pellet was dried under vacuum. To evaluate the effect of anions, experiments were performed with an ethanolic solution of $CeCl_3{\cdot}7H_2O$ but with only 30 min treatment with ozone. Similar experiments were conducted in methanol, 2-propanol, and tert-butanol with $Ce(NO_3)_3{\cdot}6H_2O$ as the cerium source for examining the effect of different alcohols on the synthesis.

2.3 Characterization methods

The morphologies, crystal structures, and chemical compositions of the different ceria NPs products were studied by bright field high resolution transmission electron microscopy (HRTEM), selected area electron diffraction (SAED), and energy dispersive X-ray spectroscopy (EDX) (FEI Tecnai Osiris S/TEM and FEI F-20 TEM both systems operated at 200 kV). The lattice structures of the NPs were also investigated using synchrotron-based powder X-ray diffraction (XRD) performed in transmission mode at the beamline BL07A of Taiwan Light Source, National Synchrotron Radiation Research Center (NSRRC). The wavelength of the monochromatic X-ray beam was selected to be 0.8266 Å. The SAED and XRD patterns of ceria samples were indexed using the ICDD card #00-004-0593 for fluorite-structured CeO_2.

The atomic structures of the as-synthesized ceria NPs and commercial bulk ceria and the chemical states of the cerium atoms were further investigated using X-ray absorption near edge spectroscopy (XANES) and extended X-ray absorption fine structure (EXAFS). The Ce L_3-edge XANES and EXAFS measurements were performed at the beamline BL07A of the Taiwan Light Source, NSRRC. A Si (111) double crystal monochromator was used to scan the photon energy under ambient conditions. The energy resolution (ΔE/E) for the incident X-ray photons was approximated to be $2.5x10^{-4}$ eV. The powder NPs sample was encapsulated by Kapton tapes and mounted onto the sample holder. The measurements were done in the transmission mode using a set of gas ionization chambers. The EXAFS spectra were analysed using the software package IFEFFIT.[10] The χ function was extracted from the raw experimental data which was then Fourier transformed into R-space. The fitting parameters for the EXAFS spectrum for the bulk ceria are shown in ESI Table S1.

The vibration modes of the ceria samples were studied using Raman spectroscopy and Fourier transformed infrared (FT-IR) spectroscopy. The Raman spectral data were obtained on a confocal Raman microscope (Horiba LabRam HR Evolution, Irvine, CA) with a 532 nm laser at an incident power of 4.5 mW. A 300 g/mm grating was employed and the spectral resolution of all spectra was ~4 cm^{-1}. FT-IR spectra were collected on a Nicolet iS50 FT-IR spectrometer (ThermoFisher Scientific, Waltham, MA). The FT-IR spectral data was measured in the transmission mode with a spectral resolution of 4 cm^{-1}. The range of the recorded FT-IR spectrum was between 500 and 4000 cm^{-1}.

The band gaps of the samples were assessed using diffuse reflective spectroscopy performed on a Shimadzu UV- 2501PC UV-Vis spectrophotometer equipped with a 60-mm integrating sphere and barium sulphate was used as the reference.

The formation of organic intermediates and by-products during the ceria NPs synthesis as well as their growth mechanism was investigated by ^{1}H-NMR on a Bruker Avance III-HD 400 MHz nuclear magnetic resonance (NMR) spectrometer. Aliquots of the reaction mixture prepared by ozonating an ethanolic cerium nitrate solution were drawn at different time intervals (15 sec, 5 min, 30 min and 1 h). These aliquots were then centrifuged and the resulting supernatant was filtered with a 0.2-µm PTFE syringe filter and diluted with $CDCl_3$. After an hour of settling, the diluted samples were passed through a 0.2-µm PTFE syringe filter again before the ^{1}H-NMR analysis.

Atomic force microscopy (AFM) was also applied to study the morphology of reaction products before separating the ceria NPs from the by-products. To prepare the AFM sample, 100 µL of the 1-hour reaction mixture prepared by ozonating an ethanolic cerium (III) nitrate solution was directly diluted to

1:100 with Nanopure water of 18 MΩ·cm. 15 µL of the diluted mixture was deposited onto a poly-*L*-lysine coated mica disc for 15 sec. The disc was then rinsed with Nanopure water for 10 sec and dried in a stream of nitrogen. The AFM sample was imaged using a Multimode Nanoscope IIIA atomic force microscope (Bruker, Santa Barbara, CA) in tapping mode with a silicon Nanosensors™ FESP probe (NanoWorld AG, Switzerland).

The catalytic activity of ceria NPs and commercial bulk ceria towards the oxidation of carbon monoxide (CO) to carbon dioxide (CO_2) was evaluated using a previously published method.[11] First, the ceria samples were activated by thermal heating in a 1"-quartz tube furnace at 400 °C for 1 hour with a flow of 30-SCCM simulated air (80% nitrogen and 20% oxygen (Matheson-Trigas, Lincoln, NE)) and an operating pressure of 0.1 Torr. Afterwards, for each activity evaluation, the activated catalysts was loaded in a U-tube reactor with a 30-SCCM flow of a gas mixture containing 1.08% CO, 20.1% oxygen and 78.82% helium (Matheson-Trigas, Lincoln, NE). The production of CO_2 at different reaction temperatures was quantified using an Agilent 7820A gas chromatograph instrument (Agilent Technologies) equipped with a thermal conductivity detector and a packed column (Alltech Hayesep Q 80/100). The longevity of ceria NPs was evaluated at 310°C for 5 h.

Results and discussion

The morphology and lattice structure of the ceria nanoparticles (ceria NPs) synthesized by the ozone-mediated methodology were studied as a function of reaction time using HRTEM and SAED. (Fig. 1 and 2) In this study, ceria NPs were prepared by ozonating an ethanolic cerium nitrate solution for 1 h. At certain time intervals (15 sec, 5 min, and 1 h), 9 µL of the solution was drawn from the reaction mixture, directly drop-casted onto a holey carbon film coated TEM copper grid and left to air dry overnight before analysis. Note that since no surfactants were used in the synthesis, the nanoparticles tended to display a high degree of aggregation on the TEM grids. The histogram of crystallite size distribution was determined by counting three hundred crystallites in the TEM images of each sample.[12] HRTEM images of these products illustrated that nanoparticles of average sizes from 2 to 4 nm were synthesized within 15 sec of ozonation. (Fig. 1 and ESI Fig. S1) The size distribution of the nanoparticles remained about the same after 5 min and even after 1 h of ozone treatment. (ESI Fig. S1). Lattice planes with a spacing of 0.31 nm, corresponding to the (111) plane of CeO_2 were often found in the HRTEM images of the ceria NPs. (Fig. 2b) SAED analysis of the diffraction ring patterns of all ceria samples indicated the products composed of fluorite-structured cerium oxide. (Fig. 1b, 1d, and 2c) The powder XRD pattern of the ceria NPs synthesized over 1 h displayed several broad diffraction lines corresponding to (111), (220), and (331) lattice planes of fluorite-structured CeO_2. (Fig. 2d) The peak broadening observed in the diffraction studies suggested the presence of small crystallites in the product.[13] The presence of

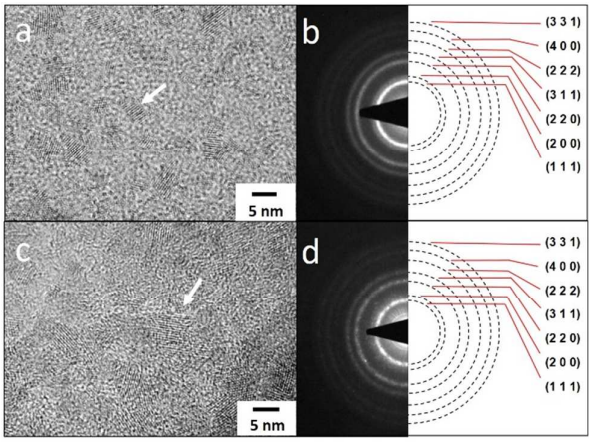

Figure 1. HRTEM images of ceria nanoparticles synthesized in (a) 15 seconds and (c) 5 minutes of ozonation. Figures 1b and 1d are corresponding SAED patterns are next to the images. White arrows indicate ceria nanoparticles.

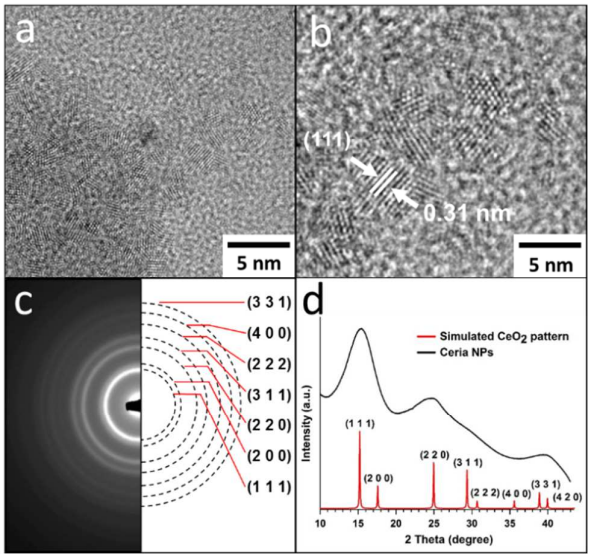

Figure 2. Ceria nanoparticles synthesized with one hour of ozonation: (a) HRTEM image, (b) zoomed-in image, (c) SAED pattern, and (d) synchrotron XRD pattern.

cerium and oxygen in the products was verified by the EDX data. (ESI Fig. S2)

The Raman spectra of the ceria NPs and the commercial bulk ceria confirmed the presence of fluorite-structured ceria in the as-synthesized particles. (Fig. 3) The most intense peaks in these spectra were at around 460 cm^{-1}, which was assigned to the F_{2g} vibration mode of fluorite-structured CeO_2.[14, 15] The position of the F_{2g} peak for the ceria NPs was red shifted (460 cm^{-1}) when compared to that of bulk CeO_2 (466 cm^{-1}). Y. Lee *et al* attributed this shift to the softening of the F_{2g} mode due to the nanosize of crystallites and an increase in oxygen vacancy.[14, 16] The nanosize of the crystallites was also indirectly revealed by the broadening of this F_{2g} peak.[2]

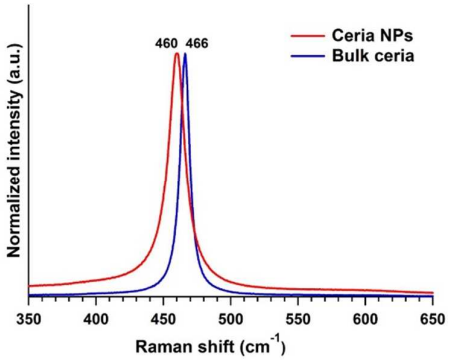

Figure 3. Raman spectra of ceria nanoparticles synthesized with one hour of ozonation and commercial bulk ceria. *The data was normalized to the peak height of the CeO_2 F_{2g} peak.

The band gap of the ceria NPs was estimated using a Tauc plot constructed from the diffuse reflectance measurements. (Fig. 4a) The diffuse reflectance data was transformed by using the Kubelka-Munk function: $F(R) = (1-R)^2/2R$, where R is the reflectance of the sample. A Tauc plot was obtained by plotting $[F(R)*h\nu]^{1/n}$ (n = 2 for indirect band gap materials such as ceria) against the photon energy.[17] The band gap of the NPs, determined by an extrapolation of a linear fit for the Tauc plot onto the energy axis, was found to be 1.9 eV. (Fig 4b) Although this value is much smaller than the band gap for bulk ceria (3.15 eV),[17] it is comparable to that of nanostructured ceria films (2.3 eV).[18] This red shift in ceria, albeit not clearly understood, had been previously attributed to both oxygen vacancies and Ce^{3+},[16] which lead to localized states in the band gap of nanosized ceria. Such states hamper the direct transition of electrons from O 2p to Ce 4f, which results in the overall narrowing of the band gap of the material.[19,20]

The percentage of Ce^{3+} in the ceria NPs was estimated from fitting the Ce L_3-edge XANES data as described by Wu *et al.*[21] A higher percentage of Ce^{3+} in the NPs (28.9 ± 0.8 %) as compared to that of the commercial bulk ceria (18.7 ± 0.1 %) was revealed in the normalized XANES analysis. (Fig. 5 and ESI Fig. S3) Nachimuthu *et al* attributed the increase in the Ce^{3+} concentration to the nanosize of prepared ceria.[22]

The local structural environment of ceria NPs was studied by comparing the Fourier transformed Ce L_3-edge EXAFS spectra of ceria NPs and bulk ceria. (Fig. 6 and ESI Fig. S4) The most significant difference between these data sets is that the R-space data of the ceria NPs shows a broad peak composed of seemingly overlapped peaks in the region between 1 Å to 2 Å. However, that of bulk ceria has only one major, narrower peak in the same region. The peaks in this region typically reflect the length of the Ce-O bond due to single-path scatterings between Ce and O. As shown in the Fourier transform magnitude data, the structural model of fluorite-structured ceria is adequate to fit the experimental EXAFS data of bulk ceria. (ESI Fig. S4 and Table S1) However, this model alone is insufficient to fit the EXAFS data of ceria NPs. Nonetheless, since our previous computation modelling results suggested that a ceria slab with 25% oxygen vacancy ($CeO_{1.5}$) can have shorter Ce-O bonds than those of the bulk (2.32 Å),[11] it is reasonable to postulate that there could be a wider range of short Ce-O bond lengths within the oxygen-deficient ceria NP samples.

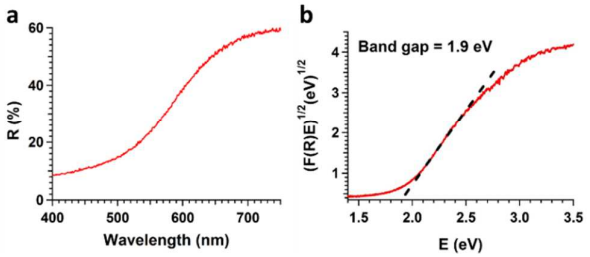

Figure 4. (a) Diffuse reflectance spectrum of ceria nanoparticles synthesized with one hour of ozonation and (b) Tauc plot of the spectrum using an indirect band gap model. The indirect band gap was estimated to be 1.9 eV. (R: Reflectance; F(R): Kubelka-Munk function; E: Photon energy)

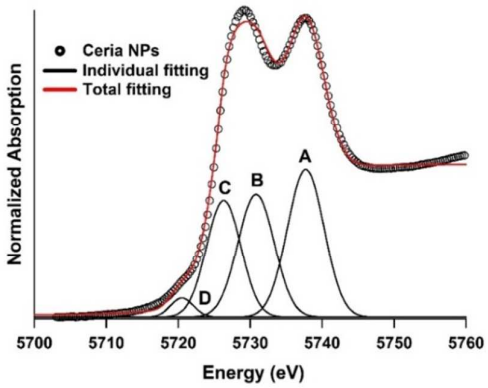

Figure 5. Ce L_3-edge XANES spectrum of ceria nanoparticles synthesized with one hour of ozonation. Peaks A and B were attributed to the Ce^{4+} state. Peak C was ascribed to the Ce^{3+} state. Peak D was due to the final states of 2p4f*. Note: 2p denotes the hole produced in $2p^{3/2}$ and 4f* indicates the presence of an excited electron in the 4f band.

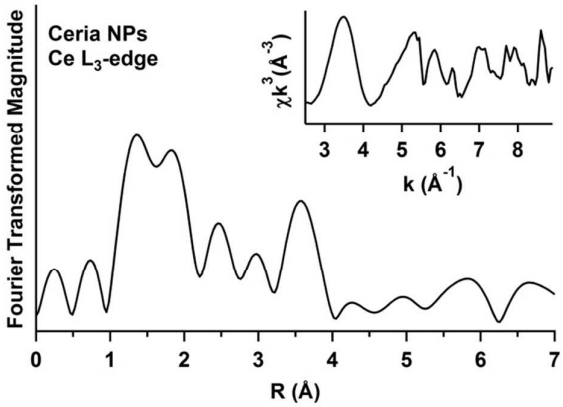

Figure 6. Fourier transformed Ce L_3-edge EXAFS spectrum of ceria nanoparticles synthesized with one hour of ozonation. (inset) Normalized data in *k*-space.

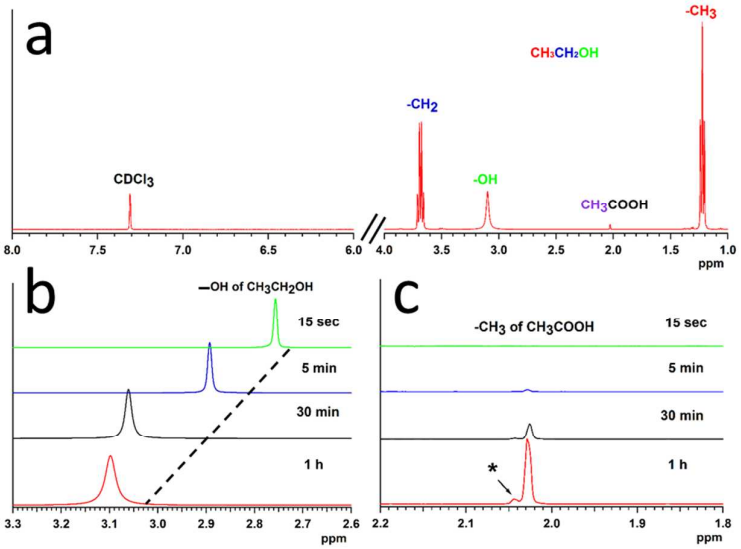

Figure 7. (a) ^{1}H NMR spectrum of an ethanol solution of cerium (III) nitrate ozonated for one hour (400 MHz, $CDCl_3$). (b) and (c) are zoomed-in regions in the ^{1}H-NMR spectra of reaction mixtures from reaction time at 15 sec, 5 min, 30 min and 1 h. Note that the asterisk in (c) represents the protons of the methyl group of ethyl acetate.

The chemical structures at the surface of the ceria NPs synthesized in ethanol were revealed using FT-IR spectroscopy. (ESI Fig. S5) Broad hydroxyl (-OH) stretching vibration bands were observed between 3100 and 3700 cm^{-1}, suggesting that the NPs were hydroxylated.[23] Weak bands ranging from 2800 to 3100 cm^{-1} were attributed to the symmetric and asymmetric stretching vibrations of methylene ($-CH_2$) and methyl ($-CH_3$) of ethyl groups at the surface.[23] Ethoxy stretching vibrations bands, characteristics of the ethanol used in the synthesis, was detected at around 900 to 1100 cm^{-1}.[24,25] The presence of stretching vibration bands of carboxylate group were also revealed at around 1200 to 1700 cm^{-1}.[26]

The versatility of this ozone-mediated synthesis of ceria NPs was studied using cerium (III) salts of different anions and different alcohol solvents. A 30-min ozonation reaction with an ethanolic solution of cerium (III) chloride was found to yield ceria NPs. (ESI Fig. S6) However, this methodology was not applicable to cerium (III) salts, such as cerium (III) sulphate and cerium (III) acetate, which have low solubility in alcohols. Besides primary alcohols such as methanol and ethanol, secondary alcohols and tertiary alcohols such as 2-propanol and tert-butanol were also successful employed to prepare NPs using this methodology. Despite using different cerium (III) salts and different types of alcohols, the size distributions of the as-synthesized ceria NPs from these syntheses were found to a range between 2 nm and 5 nm. (ESI Fig. S6 and S7)

To elucidate possible structures of intermediates during the growth of the ceria NPs, ^{1}H-NMR studies of reaction mixtures prepared by ozonating an ethanolic solution of cerium (III) nitrate were performed in $CDCl_3$ at room temperature. The NMR analysis was conducted on aliquots collected at specific time intervals (15 sec, 5 min, 30 min and 1 h). In all the four NMR spectra, prominent characteristics of the methylene group and the methyl group of ethanol, a quartet (3.69 ppm) and a triplet (1.22 ppm), were identified.[27] However, the singlet corresponding to the hydroxyl proton of ethanol, typically observed at 1.32 ppm,[27] was instead found at 2.75 ppm in the spectrum of the 15 sec sample. (Fig. 7b) The location of this singlet was further shifted from 2.75 ppm to 3.09 ppm as the reaction time increased from 15 sec to 1 h. (Fig. 7b) Since the downfield shift of hydroxyl protons has often been attributed to the complexation between the hydroxyl group and metal ions, our NMR data suggests the formation of increasingly coordinated ethanol-cerium ion intermediate complexes during the reaction.[28] As the reaction proceeds from 15 sec to 1h, the chemical shifts observed are relatively small ((3.09 - 2.75) ppm or 0.34 ppm). This can be attributed to the poorly ligating hydroxyl groups that induce a weak ligand field which results in a relatively small chemical shift compared to those observed with better donors such as acetates.[28] In addition, in these NMR spectra, a singlet at 2.02 ppm corresponding to the methyl group of acetic acid[27] was observed. (Fig. 7c) The areas under these singlets increased as the reaction time increased from 15 sec to 1 h, indicating that acetic acid was produced as a by-product as well as intermediate during the NP synthesis reaction. Other minor by-products (estimated to be < 0.1% by ^{1}H-NMR peak integration) including acetaldehyde, ethyl acetate, and acetaldehyde diethyl acetal were also observed.

Based on our characterization study of reaction intermediates and by-products and literature reports on reactions with cerium ions, we hypothesize that our reported synthesis of ceria NPs with ozone was enabled by three major chemical pathways: (1) the oxidation of alcohols into

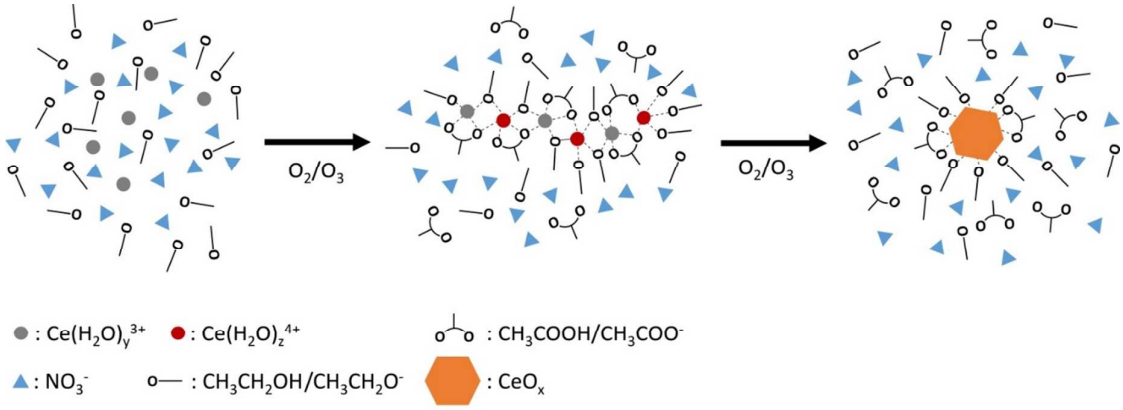

Figure 8. Schematic illustration of a possible reaction pathway for the ozone-mediated synthesis of ceria NPs in an ethanol solution of cerium (III) nitrate.

carboxylic acids mediated by ozone and cerium ions, (2) the oxidation of Ce^{3+} to Ce^{4+} by ozone in the presence of acids, and (3) the formation and decomposition of complex polymer network formed from cerium ions, alcohols, and carboxylates into ceria NPs. (Fig. 8) Using the ozonation reaction with the ethanolic cerium (III) salt solution as an example, ethanol, on being exposed to ozone, can be oxidized to acetic acid, acetate, and hydrogen peroxide.[29] The presence of acetic acid, in turn, increased the acidity of cerium (III) salt solution and promoted the oxidation of Ce^{3+} to Ce^{4+} by ozonation. This process was similar to the regeneration of Ce^{4+} by oxidation of Ce^{3+} with ozone which has been reported as a common method to decommission stainless steel and carbon steel from nuclear reactors.[30] Minor pathway for the conversion of Ce^{4+} back to Ce^{3+} in the presence of O_2 has also been reported.[31] Note that although the amount of acetic acid was too small to be observed in the ^{1}H-NMR spectrum of the 15 sec aliquot, sufficient amount of acetic acid was possibly generated in the beginning of ozonation to kick-start the oxidation of Ce^{3+} to Ce^{4+}. The generated Ce^{4+} in conjunction with ozone in turn accelerated the oxidation of ethanol to acetic acid as confirmed by the increase in acetic acid detected in longer reaction periods. (Fig. 7c)

The formation of cerium ion complexes with Ce-O linkages noted in the NMR spectra could be resulting from both the hydroxyl group of ethanol and carboxyl group of acetic acids coordinating to Ce^{4+} as well as Ce^{3+} in the reaction mixture. At the start of ozonation, Ce^{4+} and Ce^{3+} ions in the solution were likely mostly coordinated to the hydroxyl group of ethanol. Under acidic conditions, electrostatic interactions between alcohols and Ce^{4+} of ceric ammonium nitrate have been known to produce bright orange-red monomeric alcohol-Ce^{4+} ion complexes.[32, 33] The presence of these cerium ion complexes in the ceria NPs synthesis was supported by the appearance of the orange-red colour reaction mixture within the first few minutes of ozonation. (ESI Fig. S8) The acetic acid revealed in the ^{1}H-NMR study can also yield carboxylate-cerium ion complexes with Ce-O linkages. For example`, Azenha et al have shown the complexation of acetates to Ce^{3+} in an aqueous medium through detailed ^{1}H-NMR studies.[34] As the reaction proceeded, acetate ions from acetic acid competed with hydroxyl group of ethanol at binding to the cerium ions resulting in different types of Ce-O linkages.

Besides monomeric complexes, polymeric cerium ion complexes were also formed during the synthesis. The existence of polymeric species of metal ions including Bi^{3+}, Ce^{4+}, Zr^{4+} and U^{6+} in acidic aqueous conditions was verified in numerous independent studies.[35] In addition, cerium ions and carboxylate organics have been reported to form coordinated cerium polymeric species.[36] Our topographic AFM image of diluted 1-h reaction products showed the presence of ceria NPs-embedded among polymer-like species. (ESI Fig. S9) Thus, the carboxylates and hydroxyl organic species in the reaction mixture were hypothesized to cross-link the hydrated cerium ions into complex polymer networks. (Fig. 8)

The formation of crystalline ceria NPs is postulated to stem from the decomposition of the cerium ions complex polymers, which were broken down by the ozonolysis. Due to the strong electrostatic interactions between the cerium ions and the hydroxyl oxygen of ethanol or the carboxylate of the acetic acid in these complexes, the O-C bonds in these coordinated ligands are polarized and weakened, making them more susceptible to oxidation.[37] Consequently, this frees up the cerium ions to form Ce-O-Ce linkages with neighbouring cerium ions. The process is possibly similar to the formation of ceria nanodots from cerium containing polymer under UV/ozone.[9] The large lattice energy of crystalline ceria (>12,000 kJ/mol)[38] and the high oxidation power of ozone are likely the major driving forces to promote the decomposition of the cerium ion complex network to form ceria NPs products.

The 2-to-4-nm size distribution of as-synthesized ceria NPs in ethanol can also be rationalized from the functional groups detected on the surface of NPs. In the synthesis using the ethanolic cerium salt solution, ethanol and acetic acid which were known to bind onto ceria's surface, were present in the reaction mixture. The binding of these chemical species on the as-synthesized ceria NPs can be inferred by the ethoxy and carboxyl functional groups detected in our FT-IR study. In a reported synthesis of ceria nanocrystals in supercritical aliphatic alcohols,[23] alkoxide and carboxylate species have

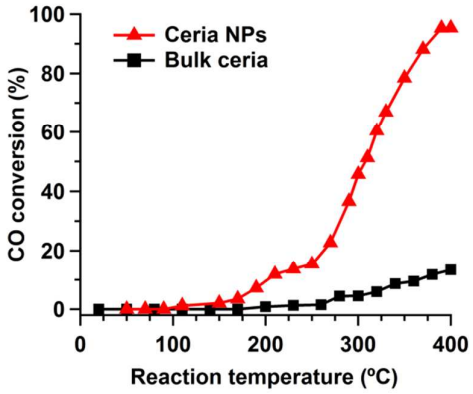

Figure 9. Comparison of the catalytic activity of ceria NPs and a commercial bulk ceria towards CO oxidation.

been postulated to modify the surface of ceria nanocrystals and limit their growth. Likely, the similar functional groups identified on our as-synthesized ceria NPs had the same effect on limiting the growth of ceria NPs into much larger particles.

The catalytic activity of ceria NPs and commercial bulk ceria was evaluated using the oxidation reaction of CO to CO_2 ($2CO + O_2 \rightarrow 2CO_2$) by measuring their light-off curves. Activation of the ceria NPs at 400 °C was necessary to facilitate the removal of organics remained on the NPs after the synthesis. The light-off temperature (T_{50}, the temperature for converting 50% of CO reactants to CO_2) for ceria NPs was determined to be *ca.* 310 °C (Fig. 9), which is comparable to those of ceria nanoparticles made by sol-gel and solvothermal processing (300 °C - 450 °C).[39] At 310 °C, the activated ceria NPs maintained its efficiency of CO conversion for at least 5 hours. (ESI Fig. S10) In contrast, the commercial bulk ceria used in this study is much less active. Its % of CO conversion reaches only about 13.4% at 400 °C. Similarly low activity has also been reported in other commercial ceria catalysts.[39, 40] Hence, our results further confirm the impact of the synthetic methods on both structural and chemical properties of ceria samples.

Conclusions

A facile, cost-effective, room-temperature synthetic method for ceria nanoparticles (NPs) was developed. Ozonation of different simple aliphatic alcohol solutions of cerium salts was demonstrated to yield fluorite-structured ceria nanoparticles with average sizes between 2 nm and 5 nm and high oxygen vacancy density. The uses of different short chain aliphatic alcohols and cerium salt precursors in these syntheses were found to have insignificant effects on the size distributions of ceria nanoparticle products. Based on the ^{1}H-NMR and AFM data, a reaction mechanism involving the formation of polymeric cerium ion complexes and their decompositions to form ceria NPs was proposed for the ozone-mediated reaction.

Conflicts of interest

There are no conflicts of interest to declare.

Acknowledgements

The authors gratefully acknowledge the financial support from National Science Foundation (CHE-1362916). We thank Johnny Goodwin from the University of Alabama for the microscopy work, Martha Morton and Thomas Smith from the University of Nebraska for their assistance in the NMR and diffuse reflectance measurements, and Max Wetherington from the Penn State University for the Raman data collection. The research was performed in part in the Nebraska Nanoscale Facility: National Nanotechnology Coordinated Infrastructure and the Nebraska Center for Materials and Nanoscience, which are supported by the National Science Foundation under Award ECCS: 1542182 and the Nebraska Research Initiative. We are also grateful to the National Radiation Research Center in Taiwan for the use of their synchrotron light source.

Notes and references

1. *Cerium oxide nanoparticles market analysis by application (energy storage, polishing agent, personal care, pharmaceuticals), by region, and segment forecasts, 2018 - 2025*, Grand View Research, Inc.: San Francisco, 2017.
2. F. H. Scholes, A. E. Hughes, S. G. Hardin, P. Lynch and P. R. Miller, *Chem. Mater.*, 2007, **19**, 2321-2328.
3. C. Sun, H. Li and L. Chen, *Energy Environ. Sci.*, 2012, **5**, 8475-8505.
4. K. K. Babitha, A. Sreedevi, K. P. Priyanka, B. Sabu and T. Varghese, *IJPAP*, 2015, **53**, 596-603.
5. G.-y. Adachi and T. Masui, in *Catalysis by ceria and related materials*, ed. A. Trovarelli, Imperial College Press: London, 2002, Vol. 2, Ch. 3, pp. 51-83.
6. A. G. DiFrancesco, R. K. Hailstone, K. J. Reed and G. R. Prok, *US Pat.,* 9340738 B2, 2016.
7. S. Barkam, J. Ortiz, S. Saraf, N. Eliason, R. McCormack, S. Das, A. Gupta, C. Neal, A. Petrovici, C. Hanson, M. D. Sevilla, A. Adhikary and S. Seal, *J. Phys. Chem. C*, 2017, **121**, 20039-20050.
8. V. P. Tolstoi and L. B. Gulina, *Russ. J. Gen. Chem.*, 2013, **83**, 1635-1639.
9. T. Ghoshal, P. G. Fleming, J. D. Holmes and M. A. Morris, *J. Mater. Chem.*, 2012, **22**, 22949-22957.
10. B. Ravel and M. Newville, *J. Synchrotron Rad.*, 2005, **12**, 537-541.
11. N. J. Lawrence, J. R. Brewer, L. Wang, T.-S. Wu, J. Wells-Kingsbury, M. M. Ihrig, G. Wang, Y.-L. Soo, W.-N. Mei and C. L. Cheung, *Nano Lett.*, 2011, **11**, 2666-2671.
12. K. An, S. Alayoglu, N. Musselwhite, K. Na and G. A. Somorjai, *J. Am. Chem. Soc.*, 2014, **136**, 6830-6833.
13. R. K. Hailstone, A. G. DiFrancesco, J. G. Leong, T. D. Allston and K. J. Reed, *J. Phys. Chem. C*, 2009, **113**, 15155-15159.
14. Y. Lee, G. He, A. J. Akey, R. Si, M. Flytzani-Stephanopoulos and I. P. Herman, *J. Am. Chem. Soc.*, 2011, **133**, 12952-12955.
15. S. Agarwal, B.L. Mojet, L. Lefferts and A. K. Datye, in *Catalysis by Materials with Well-Defined Structures*, eds. Zili Wu and S. H. Overbury, Elsevier Science, 2015, Ch. 2, pp. 31-70.

16. B. Choudhury, P. Chetri and A. Choudhury, *RSC Adv.*, 2014, **4**, 4663-4671.
17. B. Choudhury and A. Choudhury, *Mater. Chem. Phys.*, 2012, **131**, 666-671.
18. T. M. Inerbaev, A. S. Karakoti, S. V. N. T. Kuchibhatla, A. Kumar, A. E. Masunov and S. Seal, *Phys. Chem. Chem. Phys.*, 2015, **17**, 6217-6221.
19. P. Patsalas, S. Logothetidis, L. Sygellou and S. Kennou, *Phys. Rev. B*, 2003, **68**, 035104.
20. B. Tatar, E. D. Sam, K. Kutlu and M. Ürgen, *J. Mater. Sci.*, 2008, **43**, 5102-5108.
21. T.-S. Wu, Y. Zhou, R. F. Sabirianov, W.-N. Mei, Y.-L. Soo and C. L. Cheung, *Chem. Commun.*, 2016, **52**, 5003-5006.
22. P. Nachimuthu, W.-C. Shih, R.-S. Liu, L.-Y. Jang and J.-M. Chen, *J. Solid State Chem.*, 2000, **149**, 408-413.
23. C. Slostowski, S. Marre, O. Babot, T. Toupance and C. Aymonier, *Langmuir*, 2012, **28**, 16656-16663.
24. B. Giroire, C. Slostowski, S. Marre, C. Aymonier, T. Aida, D. Hojo, N. Aoki, S. Takami and T. Adschiri, *Phys. Chem. Chem. Phys.*, 2016, **18**, 1727-1734.
25. M. Li, Z. Wu and S. H. Overbury, *J. Catal.*, 2013, **306**, 164-176.
26. C. Slostowski, S. Marre, O. Babot, T. Toupance and C. Aymonier, *Langmuir*, 2014, **30**, 5965-5972.
27. G. R. Fulmer, A. J. M. Miller, N. H. Sherden, H. E. Gottlieb, A. Nudelman, B. M. Stoltz, J. E. Bercaw and K. I. Goldberg, *Organometallics*, 2010, **29**, 2176-2179.
28. C.-H. Huang and J. R. Morrow, *Inorg. Chem.*, 2009, **48**, 7237-7243.
29. A. W. Wright, *Am. J. Sci.*, 1874, **7**, 184-188.
30. S. Singh, A. N. Bhaskarwar, T. Vincent and P. K. Wattal, *J. Radioanal. Nucl. Chem.*, 2016, **309**, 691-700.
31. G. Zhou, B. Gui, H. Xie, F. Yang, Y. Chen, S. Chen and X. Zheng, *J. Ind. Eng. Chem. Res.*, 2014, **20**, 160-165.
32. F. R. Duke and G. F. Smith, *Ind. Eng. Chem. Anal. Ed.*, 1940, **12**, 201-203.
33. L. B. Young, Ph.D. thesis, Iowa State University, 1968.
34. M. E. Azenha, H. D. Burrows, S. M. Fonseca, M. L. Ramos, J. Rovisco, J. S. de Melo, A. J. F. N. Sobral and K. Kogej, *New J. Chem.*, 2008, **32**, 1531-1535.
35. E. L. King and M. L. Pandow, *J. Am. Chem. Soc.*, 1952, **74**, 1966-1969.
36. I. L. Malaestean, M. Kutluca-Alıcı, A. Ellern, J. van Leusen, H. Schilder, M. Speldrich, S. G. Baca and P. Kögerler, *Cryst. Growth Des.*, 2012, **12**, 1593-1602.
37. Q. Wang, L. Ye, Y. Yang, X. Lv and J. Lu, in *Software engineering and knowledge engineering: Theory and practice. Selected papers from 2012 International Conference on Software Engineering, Knowledge Engineering and Information Engineering (SEKEIE 2012)*, ed. W. Zhang, Springer, 2012, pp. 169-175.
38. S. Ohmi, S. Akama, A. Kikuchi, I. Kashiwagi, C. Ohshima, J. Taguchi, H. Yamamoto, C. Kobayashi, K. Sato, M. Takeda, K. Oshima, H. Ishiwara and H. Iwai, in *Extended Abstracts of International Workshop on Gate Insulator. IWGI 2001 (IEEE Cat. No.01EX537)*, IEEE, 2001, pp. 200-204.
39. J. Yang, L. Lukashuk, H. Li, K. Föttinger, G. Rupprechter and U. Schubert, *Catal. Lett.*, 2014, **144**, 403-412.
40. M. Lykaki, E. Pachatouridou, E. Iliopoulou, S. A. C. Carabineiro and M. Konsolakis, *RSC Adv.*, 2017, **7**, 6160-6169.

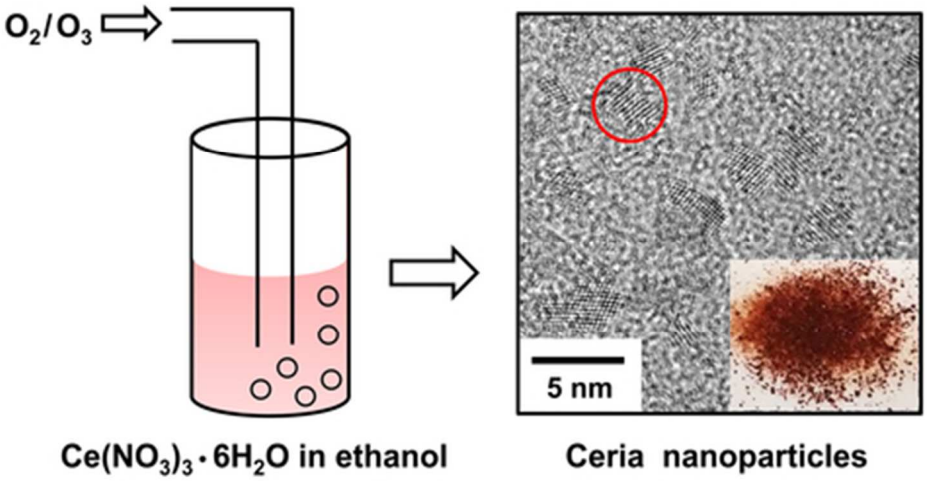

43x23mm (300 x 300 DPI)